Mimetic Divergence and the Speciation Continuum in the Mimic Poison Frog *Ranitomeya imitator*

Evan Twomey,[1,2,*] Jacob S. Vestergaard,[3] Pablo J. Venegas,[4] and Kyle Summers[1]

1. Department of Biology, East Carolina University, Greenville, North Carolina 27858; 2. Laboratório de Sistemática de Vertebrados, Pontifícia Universidade Católica do Rio Grande do Sul (PUCRS), Avenida Ipiranga 6681, Porto Alegre, 90619-900, Brazil; 3. Department of Applied Mathematics and Computer Science, Technical University of Denmark, Kongens Lyngby 2800, Denmark; 4. División de Herpetología, Centro de Ornitología y Biodiversidad (CORBIDI), Calle Santa Rita 105, Oficina 202, Urbanización Huertos de San Antonio, Surco, Lima, Peru

Submitted January 8, 2015; Accepted July 20, 2015; Electronically published December 9, 2015

Online enhancements: appendix. *Dryad data:* http://dx.doi.org/10.5061/dryad.95tv3.

abstract: While divergent ecological adaptation can drive speciation, understanding the factors that facilitate or constrain this process remains a major goal in speciation research. Here, we study two mimetic transition zones in the poison frog *Ranitomeya imitator*, a species that has undergone a Müllerian mimetic radiation to establish four morphs in Peru. We find that mimetic morphs are strongly phenotypically differentiated, producing geographic clines with varying widths. However, distinct morphs show little neutral genetic divergence, and landscape genetic analyses implicate isolation by distance as the primary determinant of among-population genetic differentiation. Mate choice experiments suggest random mating at the transition zones, although certain allopatric populations show a preference for their own morph. We present evidence that this preference may be mediated by color pattern specifically. These results contrast with an earlier study of a third transition zone, in which a mimetic shift was associated with reproductive isolation. Overall, our results suggest that the three known mimetic transition zones in *R. imitator* reflect a speciation continuum, which we have characterized at the geographic, phenotypic, behavioral, and genetic levels. We discuss possible explanations for variable progress toward speciation, suggesting that multifarious selection on both mimetic color pattern and body size may be responsible for generating reproductive isolation.

Keywords: mimicry, ecological speciation, landscape genetics, mate choice, approximate Bayesian computation.

Introduction

Divergent selection among populations inhabiting different ecological conditions has been shown to generate reproductive isolation (Hatfield and Schluter 1999; Jiggins et al. 2001; Nosil et al. 2003; McKinnon et al. 2004; Chamberlain et al. 2009), a process known as ecological speciation (Schluter 1996; Nosil 2012). Despite wide appreciation for the role of divergent adaptation in speciation, our understanding of the factors that promote or inhibit incipient population divergence remains limited. Studies have found that, while divergent selection can often initiate speciation, there is substantial variability among natural systems in how far speciation has progressed (Funk et al. 2006; Rosenblum 2006; Mallet et al. 2007; Hendry et al. 2009; Nosil et al. 2009; Seehausen 2009; Merrill et al. 2011; Rosenblum and Harmon 2011). This variability in stage of speciation is often referred to as the "speciation continuum," and a major goal in speciation research is to understand the conditions that influence progress along this continuum.

Comparative studies based on natural replicates of population divergence offer a powerful approach for understanding the conditions that facilitate or constrain ecological speciation (Jiggins et al. 2004; Rosenblum 2006; Berner et al. 2009; Rosenblum and Harmon 2011). One approach involves studying multiple species that have diverged across a common ecological setting, revealing inherent properties of species that facilitate or constrain ecological speciation. For example, in a study of replicated ecological divergence of three lizard species across a common ecological gradient (a white sands/dark soil ecotone), Rosenblum and Harmon (2011) found that population divergence was strongest in a habitat-specialist species with low dispersal rates and weakest in a generalist species with high dispersal rates, suggesting that variation in dispersal rates among species may explain differential progress toward speciation. Alternatively, by studying a single species (or species pair) that has undergone replicated divergence across a range of ecological settings, we can understand how ecological differences can facilitate or constrain speciation (Jiggins et al. 2004; Berner et al. 2009; See-

* Corresponding author; e-mail: evan.twomey@gmail.com.

Am. Nat. 2016. Vol. 187, pp. 205–224.
DOI: 10.1086/684439

hausen 2009). A good example of this approach is the cichlid species pair *Pundamilia pundamilia* and *Pundamilia nyererei*, in which reproductive isolation between the two species increases with increasing water clarity (Seehausen et al. 2008; Seehausen 2009). By identifying additional examples of replicated ecological divergence, we can better understand the properties of species and environments that are conducive to ecological speciation.

Hybrid zones (also referred to as contact zones, transition zones, or clines, depending on the context) have been important for speciation research, as they often reflect a balance between the diversifying effects of local adaptation and the homogenizing effects of gene flow and migration (Barton and Hewitt 1985). Because hybrid zones occur between species or populations that can still exchange genes, they provide insight into reproductive barriers that arise early in the process of speciation. Three general mechanisms are thought to produce stable clines: (1) environmental ecotones, (2) heterozygote disadvantage, and (3) positive frequency dependence (Haldane 1948; Endler 1977; Szymura and Barton 1986; Mallet and Barton 1989). A cline formed from an ecotone reflects local adaptation of a single species to distinct, abutting environments (e.g., the White Sands lizards mentioned above). In a cline formed by heterozygote disadvantage, selection against recombinants in the zone center acts as a hybrid sink, which can slow gene flow between parental forms (Barton and Hewitt 1985). Finally, positive frequency-dependent selection can lead to stable clines between distinct forms. As with clines formed by heterozygote disadvantage, clines based on positive frequency dependence are not regulated by external environmental factors and thus may move over time (Barton and Hewitt 1985).

Aposematic signals represent a clear example of a trait that is under frequency-dependent selection (Endler and Greenwood 1988; Greenwood et al. 1989). Signals under positive frequency dependence are predicted to be uniform (Joron and Mallet 1998), bringing into question the initial source of signal divergence among populations. In certain cases, such as Müllerian mimicry, signal divergence is predicted if different populations are subject to selection to resemble different model species. Thus, Müllerian mimicry is an intriguing mechanism driving population divergence, in that we frequently observe (1) signal uniformity within populations and (2) signal divergence between populations. Divergence in mimicry appears to be responsible for speciation in the *Heliconius* butterflies in many cases (Jiggins 2008) and may also have driven speciation in certain groups of reef fish (Puebla et al. 2007). The dendrobatid poison frog *Ranitomeya imitator* is a Müllerian mimic (Symula et al. 2001; Stuckert et al. 2014*a*, 2014*b*) that has undergone rapid diversification in color pattern to establish four distinct morphs in north-central Peru (Twomey et al. 2013). Based on previous research (Yeager 2009; Yeager et al. 2012; Twomey et al. 2013) and ongoing fieldwork, a relatively clear geographic picture of the *R. imitator* mimicry system is emerging. There are four mimetic morphs of *R. imitator*, each of which resembles a distinct model species (fig. 1). The geographic distributions of each morph appear to form a mosaic, with narrow transition zones forming where mimetic morphs come into contact. Thus far we have found three such transition zones (fig. 1), all of which involve a transition between the striped morph and some other morph. The mimetic radiation of *R. imitator* represents an excellent system in which to study the role of mimicry in speciation for several reasons. First, the initial source of mimetic divergence is relatively clear, in that various morphs of a single species have diverged to resemble different model species. Second, all the mimetic morphs belong to a single species; thus, we can study reproductive barriers that arise in the earliest stages of population divergence. Third, there is replicated ecological divergence in *R. imitator*, in that there are three known instances of mimetic divergence between the striped morph and another morph. Fourth, different mimetic morphs appear to have undergone varying levels of morphological divergence, which allows us to address whether the strength or diversity of color pattern divergence is positively correlated to the strength of reproductive isolation.

The main purpose of this article is to study two mimetic transition zones in *R. imitator* to address whether mimetic divergence is driving reproductive isolation between different mimetic morphs. Specifically, we characterize the extent of mimetic, genetic, and behavioral divergence across these transition zones. In a previous study (Twomey et al. 2014*a*), we used a combination of color pattern quantification, cline analysis, mate choice experiments, and landscape genetics to study reproductive isolation across the striped-varadero transition zone. In that study, we found that mimetic divergence appears to have led to a breakdown in gene flow between morphs, possibly facilitated by assortative mating, which is consistent with the idea that mimetic divergence is driving ecological speciation in this system. In this study, we use the same methods to study two additional transition zones (banded-striped and spotted-striped; fig. 1) to determine whether mimetic divergence has led to reproductive isolation more generally. From earlier results, if mimetic divergence is driving reproductive isolation, we predict that (1) phenotypic clines should be relatively narrow (<4 km), (2) mimetic morphs should demonstrate genetic divergence (above what is predicted by geographic distance alone), and (3) different mimetic morphs should exhibit mating preferences toward their own morph. As we now have data on three independent cases of mimetic divergence within a single species, we can compare all three transition zones, which allows us to investigate the factors explaining differential progress toward speciation.

Methods

The methods of this article largely follow those of Twomey et al. (2014*a*). That study focused on a single mimetic transition zone in *Ranitomeya imitator*. Here, we focus on two additional transition zones. Therefore, for consistency and to facilitate direct comparisons among all three transition zones, the description of the methods here closely follows that in Twomey et al. (2014*a*). All data are deposited in the Dryad Digital Repository: http://dx.doi.org/10.5061/dryad.95tv3 (Twomey et al. 2016).

Sample Collection and Description of Transects

For the color pattern analysis across the banded-striped transect, we sampled 125 *R. imitator* from 11 localities in the departments of San Martín and Loreto, Peru (table A1; tables A1–A7 available online). These localities form a roughly southwest-northeast linear transect along the Huallaga River (fig. 1), approximately from the town of Sauce, in San Martín, to the lowlands near the city of Yurimaguas. For genetic analyses, we sampled 158 *R. imitator* from 11 localities. We included an additional 91 samples from 11 localities from Twomey et al. (2013) and 36 samples from one locality from Twomey et al. (2014*a*), for a combined data set of 285 individuals from 16 localities (table A1). We calculated transect position for each sampling locality as the straight-line distance from the estimated center of the transition zone. Localities southwest of this point were given a negative sign and those northeast of this point a positive sign. The initial center point (latitude −6.5584°, longitude −75.9517°) used in this calculation was based on field observations where an apparent shift in color pattern occurred. Therefore, in our cline analyses, center estimates close to 0 indicate that the inferred cline center was consistent with our field observations. For details on cline fitting, see appendix, available online.

For the color pattern analysis of the spotted-striped transect, we sampled a total of 140 *R. imitator* from eight localities in San Martín and Loreto (table A2). With the exception of the Pinto Recodo locality, these localities form a roughly linear transect running south to north, extending approximately from the city of Tarapoto to the lowlands near the city of Yurimaguas. For the genetic analysis of this transect, we sampled 82 *R. imitator* from seven localities. In addition, we included 33 samples from three localities from Twomey et al. (2013) and 36 samples from one locality from Twomey et al. (2014*a*), for a combined data set of 151 individuals from eight localities (table A2). As with the previous transect, we calculated transect position for sampling localities as the straight-line distance from an estimated transition zone center (for the spotted-striped transect, this center point was −6.3629°, −76.2939°).

We also took color pattern measurements from the following model species and populations: seven individuals of lowland *Ranitomeya variabilis* from Pongo de Cainarachi (the model for the striped morph of *R. imitator*), seven individuals of highland *R. variabilis* from San Jose (the model for the spotted morph of *R. imitator*), and six individuals of *Ranitomeya summersi* from Sauce (the model for the banded morph of *R. imitator*).

Color and Pattern Data

Frog color (hue and brightness) was quantified by measuring the spectral reflectance at specific points on the dorsum of each frog. One measurement was taken on each side (i.e., right and left) of the head, mid-body, and rear-body and the dorsal surfaces of the right and left thighs, for a total of eight spectral-reflectance measurements per frog. Spectral-reflectance measurements were taken with an Ocean Optics USB4000 spectrometer equipped with a LS-1 tungsten-halogen light source and Ocean Optics Spectrasuite software. We used a black plastic tip on the end of the probe to ensure that measurements were taken at a consistent distance (3 mm) and angle (45°) relative to the skin. To account for lamp drift, we measured a white reflectance standard (Ocean Optics WS-1-SL) after every other frog. Raw spectra were processed in AVICOL software, version 6 (Gomez 2006), using Endler's segment model (Endler 1990) calculated between 450 and 700 nm. This model calculates brightness (Qt), chroma (C), hue (H), brightness in the yellow-blue range, and brightness in the red-green range. After processing in AVICOL, readings were averaged within body regions (head, body, and legs).

To quantify pattern, we used dorsal photographs and an automated feature extraction method to extract a suite of pattern descriptor variables. All photos were taken on a white background with a Canon Rebel XS digital single-lens reflex camera equipped with a Canon EF 100-mm macro lens and the camera flash. Image descriptors were automatically extracted from images of every individual and collected in a feature matrix. We extracted three types of descriptors: color/noncolor ratio, gradient orientation histograms, and shape index histograms (Koenderink and van Doorn 1992; Dalal and Triggs 2005; Larsen et al. 2014). These descriptors capture zeroth-, first-, and second-order image structure, respectively. We used a spatial pooling scheme to collect information separately at four interest points: left leg, right leg, posterior dorsum, and anterior dorsum. At each of these interest points, pattern variation occurs on a distinct scale, so the descriptors were extracted according to a scale-space formulation (Lindeberg 1996). Color/noncolor ratios were extracted for every interest point on a single scale, gradient orientation histograms for every interest point on two different scales and two orientation bins (horizontal and vertical), and shape index histograms were extracted for the legs on two

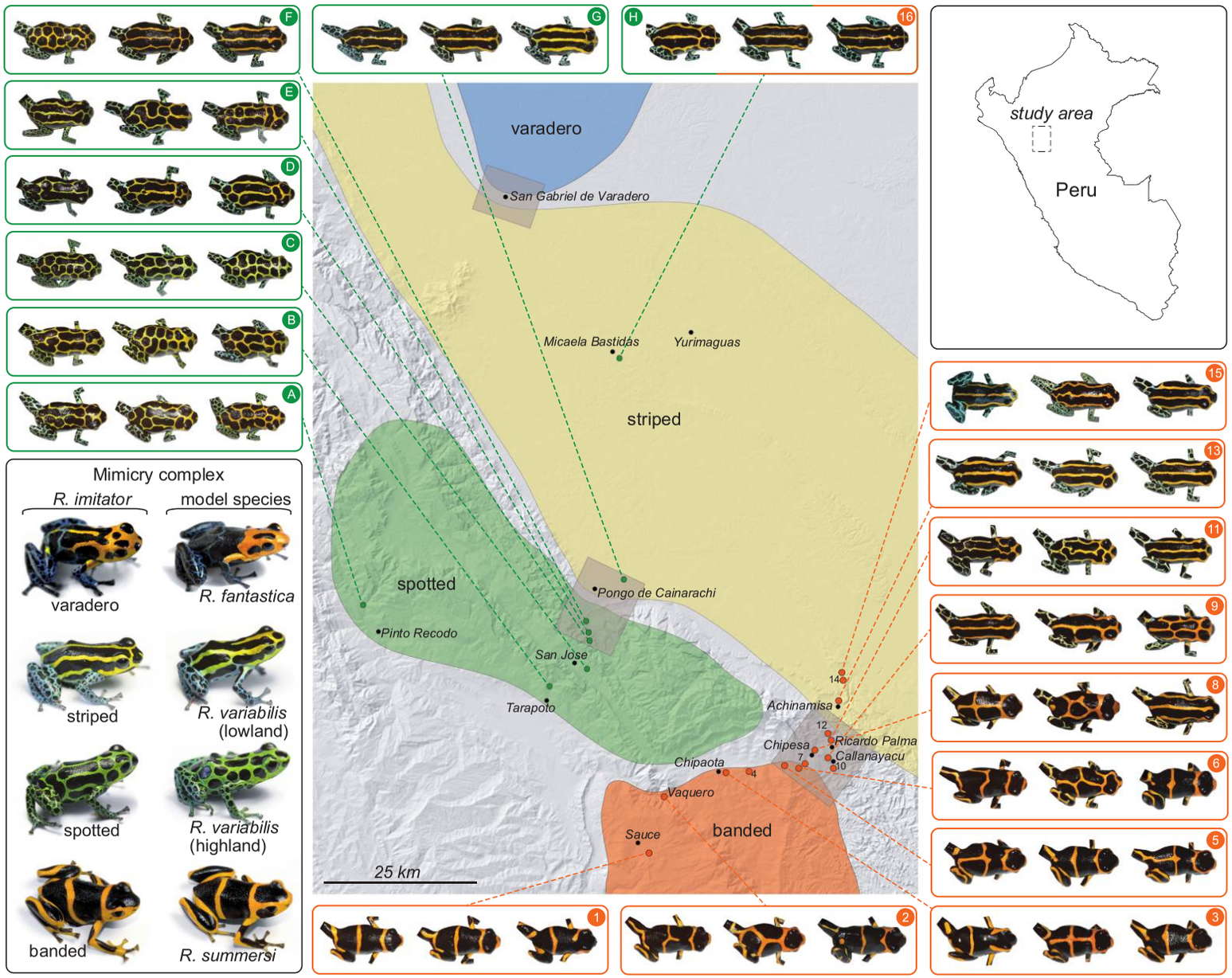

scales in five bins equidistantly spaced between $-\pi/2$ and $\pi/2$. This sums to a total of $4 \cdot (1 + 2 \cdot 2 + 2 \cdot 5) = 60$ features per individual.

To reduce the multivariate color and pattern data to a single descriptive metric for each body region, we used kernel discriminant analysis (Mika et al. 1999), with individuals of the model species representing the training groups used for classification. In both sampling transects, the phenotypic transition in *R. imitator* involves a shift from the striped morph (which mimics lowland *R. variabilis*) to either the spotted morph (which mimics highland *R. variabilis*) or the banded morph (which mimics *R. summersi*). Therefore, for the spotted-striped transect, the populations of the model species used for classification were highland *R. variabilis* and lowland *R. variabilis*; for the banded-striped transect, the model species used were *R. summersi* and lowland *R. variabilis*. This procedure assigns a discriminant score to each *R. imitator* individual on the basis of its similarity to either model species and thus can be thought of as a mimicry score. The analysis can be constrained to include only subsets of the variables to derive separate color and pattern metrics for different parts of the body. We derived color and pattern metrics for two body regions: dorsum and legs. The multivariate color and pattern data are high-dimensional representations of the individuals, compared to the number of individuals, wherefore we introduced regularization of the solution, adjusted by the regularization parameter λ. Kernel methods represent the multivariate observations by the interobservation distances, defined by a kernel. We used a Gaussian kernel with width γ (table A3). The parameters λ and γ were selected to minimize the intralocation variance of the *R. imitator* discriminant scores while keeping them within the range of the model species' discriminant scores. The formulation of kernel discriminant analysis makes it impossible to inspect the loadings as one would do in linear discriminant analysis to determine variable importance. To determine which variables were relevant for the discriminant analysis, we calculated the mutual information between each of the original variables $\{\mathbf{x}_1, \ldots, \mathbf{x}_p\}$ and the discriminant scores (metric) $\mathbf{z}$. Mutual information (MI) is defined as

$$\mathrm{MI}(x, y) = \frac{H(x) + H(y) - H(x, y)}{H(x) + H(y)},$$

where $H(x)$ and $H(x, y)$ are marginal and joint entropies, respectively. Entropy is a measure of the amount of information contained in a signal, and MI is a measure of the similarity between two such signals or variables. To estimate the entropy of a signal, the probability distribution of the signal must be estimated; for this purpose we used kernel density estimation (also known as Parzen windows). The MIs between the variables were used to define each of the six metrics, and the resulting metric can be seen in figures A1 and A2 (figs. A1–A8 available online). The values $\mathrm{MI}(\mathbf{x}_i, \mathbf{z})$ are normalized such that $\mathrm{MI}(\mathbf{x}_i, \mathbf{x}_i) = \mathrm{MI}(\mathbf{z}, \mathbf{z}) = 1$.

Landscape Genetics

Tissue samples for genetic analysis (toe clips) were taken with sterile surgical scissors and preserved in 96% ethanol before extraction. We amplified the following microsatellite loci: RimiA06, RimiA07, RimiB01, RimiB02a, RimiB07, RimiB11, RimiC05a, RvarD01, RimiD04, RimiE02a, and RimiF06, following extraction and amplification protocols described in Brown et al. (2009), with the exception that 56°C was used as the annealing temperature for RimiB07, RimiC05a, and RimiE02a and 54°C was used for RvarD01. Forward primers were labeled with a fluorescent tag for visualization (6-FAM, NED, PET, or VIC). Loci were amplified individually and multiplexed for sequencing. Sequencing was done on an ABI 3130 sequencer, and fragment sizes were analyzed with GeneMapper software (Applied Biosystems). We used MICRO-CHECKER software, version 2.2.3 (van Oosterhout et al. 2004), to check for the presence of null alleles. One locus (RimiE02a) showed evidence for high null-allele frequencies (mean across populations > 0.10), and this locus was omitted from further analyses. Another locus (RimiB01) did not amplify for most of the banded populations and was omitted from the banded-striped transect analysis.

We used the program Structure, version 2.3.4 (Pritchard et al. 2000), to investigate population genetic structure along each transect from the microsatellite data. This program employs a Bayesian clustering algorithm to assign individuals probabilistically to each of K populations, where K, the number of populations, is unknown. The program was run with a burn-in of 50,000 generations and 500,000 subsequent generations for one to five genetic clusters

Figure 1: Müllerian mimicry and variation in *Ranitomeya imitator*. Lower left: Depiction of the mimicry complex, showing four mimetic morphs of *R. imitator* and corresponding model species. Upper right: Map of Peru showing study area. Center: geographical distribution of mimetic morphs of *R. imitator* and sampling localities. Orange dots show *R. imitator* populations included on the banded-striped transect; green dots show *R. imitator* populations included on the spotted-striped transect; black dots represent towns. Population numbers/letters correspond to tables A1 and A2, available online, respectively. Note that the Micaela Bastidas population (population H/16) is included in both transects. The gray boxes show the three mimetic transition zones studied here. Note that the spotted and banded morphs come into close contact but do not form a transition zone, which is apparently due to geographic isolation from the Huallaga River.

($K = 1$–5), with five replicates at each value of K. The program used the admixture model with correlated allele frequencies. No prior information on sampling location was used in the model. To determine the number of clusters that best describe the data, we used the method described in Evanno et al. (2005), which is based on the second-order rate of change of the log likelihood. This method was implemented in Structure Harvester (Earl and vonHoldt 2012).

We conducted landscape genetic analyses to quantify the relative effects of geographic distance and color pattern distance on genetic distance between populations. Under an isolation-by-distance (IBD) scenario, geographic distance alone will account for much of the observed genetic distance between populations. If mimetic divergence is also an isolating barrier (i.e., isolation by adaptation, or "IBA," which would be expected under morph-based reproductive isolation), then population-wise mimetic divergence should also account for a significant proportion of the observed genetic distance between populations. We used a multiple-matrix regression method (Wang 2013) in order to quantify the relative effects of two distance matrices (geographic distance and color pattern distance) on the genetic-distance matrix. This method incorporates multiple regression, such that the relative effects of two or more predictor variables on genetic distance can be quantified, as can the overall fit of the model. Results consist of regression coefficients (β) and associated P values. Regression coefficients here are denoted β_{D} (for geographic distance) and β_{CP} (for color pattern distance) and are thus measures of the relative importance of IBD and IBA, respectively. We ran the multiple-matrix regression analyses with 10,000 permutations, using the R script provided in Wang (2013). Our distance matrices consisted of one measure of geographic distance (Euclidean distance), one measure of genetic distance (Nei's D), and one measure of color pattern distance (difference in discriminant score; see below). For the geographic-distance matrix, we calculated pairwise straight-line distance between populations. For the genetic-distance matrix, we calculated Nei's D between all pairs of populations in GENALEX, version 6.5 (Peakall and Smouse 2006). To generate the color pattern distance matrix, we calculated pairwise differences in population mean discriminant scores from the kernel discriminant function analysis. Because this analysis takes into account features of the model species, it can be thought of as a composite difference in mimetic color pattern. We conducted landscape genetic analyses separately for each transect.

To estimate cline shape for the microsatellite data on each transect, we used the first major axis from a factorial-correspondence analysis (FCA) calculated with the software GENETIX, version 4.5 (Belkhir et al. 1996). This method is conceptually similar to principal-components analysis, except that it takes into account features of genetic data such as heterozygosity and homozygosity. The program was run without any prior population information on the samples.

Divergence-Time Estimates Using Approximate Bayesian Computation

As the amount of reproductive isolation between population pairs should increase with time since divergence, we estimated divergence times between morphs to determine whether this could explain variation in reproductive isolation. To do this, we used approximate Bayesian computation (ABC) in the program DIYABC 2.0.4 (Cornuet et al. 2008, 2014). This program simulates coalescent-based data sets, which are then summarized using a set of summary statistics and compared to the observed data set. Our goals for this analysis were (1) to estimate the relative likelihoods of different demographic scenarios and (2) to estimate parameters (i.e., divergence times) for the best-supported demographic scenarios. For this analysis, we used a reduced microsatellite data set containing the following four populations, representing the "pure" mimetic morphs: Micaela Bastidas (striped morph), Sauce (banded morph), San Jose (spotted morph), and Varadero (varadero morph; data from Twomey et al. 2014*a*). We tested 31 possible topologies, seven of which contained recent admixture events to account for ongoing gene flow between populations. For the initial analysis, we tested five groups of five scenarios each and one group with six scenarios, simulating 500,000 data sets for each scenario. Scenarios were assigned to groups randomly. Within each group, posterior probabilities of scenarios were calculated with the logistic-regression approach, with 2% of the subsets of the closest simulated data (Cornuet et al. 2008). We then ran a second analysis, where we tested the six best scenarios (as identified from the first analysis; fig. A3) against each other, simulating 1 million data sets per scenario. All scenarios used in these analyses are available in the Dryad Digital Repository: http://dx.doi.org/10.5061/dryad.95tv3 (Twomey et al. 2016). Scenarios used a single parameter for effective population size, 1–3 parameters estimating divergence times, and an admixture rate parameter (in admixture scenarios). Details on priors, summary statistics, model checking, and parameter estimation are given in the appendix.

Mate Choice: Free-Release Trial Protocols and Statistical Analysis

For details on mate choice collecting localities and animal husbandry, see the appendix. To test for morph-based mating preferences, we conducted triad mate choice experiments, in which we introduced two females (one of each morph) into the terrarium of a given male and measured the amount of courtship time between the male and the

same-morph female versus that between the male and the alternate-morph female. In *R. imitator*, courtship starts when a calling male approaches a female. The female can reciprocate interest by following the male to an oviposition site while the male continues calling, or she can otherwise show no interest (Brown et al. 2008*a*). Our mate choice experiments facilitated these behaviors in that a male was free to initiate courtship with either female and the female was free to reciprocate interest or reject the male. Initiation of courtship is readily observable in captivity, as males produce a rapid courtship call and/or begin to walk with a staccato-like rhythm in the vicinity of the female. Therefore, when a male displayed either of these behaviors near a female, this marked the initiation of courtship. Courtship was judged to have ended under either of the following conditions: (1) the male moves away and the female does not respond, or (2) the female moves away and the male does not respond. Using these criteria, we measured in each trial the total amount of courtship time between the male and each female. These trials were initiated by placing two females into the terrarium of a male at the same time. Trials were filmed for 1 h. After the trial, the same females were then released into a terrarium of a male of the other morph and again filmed for 1 h (see below for justification of paired-samples design). To account for any order effects, the morph of the male tested first was randomly selected. In cases where the male or one or more females were unresponsive (e.g., by hiding in the gravel), trials were repeated at a later date. Terraria were illuminated with a full-spectrum ZooMed AvianSun 5.0 UVB 26-W compact fluorescent bulb. To allow the full spectrum of light into the terrarium, we used a custom-built terrarium cover made of ultraviolet-transparent acrylic.

Although it would have been desirable to match the two females for mass, this was not feasible because of substantial mass differences among populations. For example, the allopatric striped population has an average female mass of 0.56 g (Twomey et al. 2014*a*), whereas the allopatric banded population has an average female mass of 0.65 g ($n = 14$). To control for differences between females, we used a paired-samples experimental design whereby a given pair of females was presented to a male of each morph. This design addresses the question of how changing male morph type alters courtship probabilities when female identity is held constant.

To analyze the free-release mate choice data, we used generalized linear mixed models (GLMMs) in the glmmADMB package (Skaug et al. 2011) in R, version 3.0.2 (R Development Core Team 2005), with an underlying beta-binomial error distribution to test whether the time males spent courting each female morph was influenced by male population origin. We used "male origin" as a fixed effect and "pair ID" (i.e., a unique identifier assigned to each female pair) as a random effect to account for the paired-samples experimental design. The significance of male origin was determined with χ^2 tests comparing models where male origin was either included or excluded as a parameter.

For the banded-striped transition zone, we essentially ran two distinct experiments: one where frogs originated from allopatric populations and one where frogs originated from transition zone (parapatric) populations. In the former experiment, frogs originated from Sauce (allopatric banded) or Micaela Bastidas (allopatric striped); in the latter experiment, frogs originated from Chipaota (transition zone banded) or Achinamisa (transition zone striped; fig. 1). Because of this design, it is not appropriate to make direct comparisons between two populations of the same morph because male origin is confounded with female origin (i.e., it is not possible to assign variation in preference strength to male origin, as females came from different sites in the different experiments). Therefore, our design allowed for two comparisons: allopatric banded versus allopatric striped and transition zone banded versus transition zone striped. Under a scenario where mate preferences have diverged in allopatry, we expect allopatric populations to show stronger assortative mating than transition populations. Alternatively, if mate preferences are enhanced at the transition zone (e.g., because of reinforcement), we expect that assortative mating should be strongest between the two transition populations. Here, we ran two separate GLMMs, one for each experiment.

For the spotted-striped transition zone, because we used a single spotted population for mate choice trials, our experiment addresses whether preferences in the allopatric striped population (Micaela Bastidas) and the transition zone striped population (Pongo) are different from each other. This design also allows us to address preferences in the spotted population under two conditions: when the striped female was from a transition zone population and when the striped female was from an allopatric population. For this experiment, we ran a single overall GLMM (i.e., across all three populations).

To assess whether color pattern alone mediates assortative mating, we ran mate choice experiments using plastic frog models painted with banded or striped color patterns. Here, we tested only male preference, as females typically reacted aggressively toward plastic models. For details on the plastic-model experiments, see the appendix.

Results

Color Pattern and Microsatellite Cline Analysis: Banded-Striped Transect

For the banded-striped transect, we found evidence of a sigmoidal cline in all four color pattern metrics (dorsal color, dorsal pattern, leg color, and leg pattern; figs. 2, A4*a*; table A6). Moving along the transect from the banded

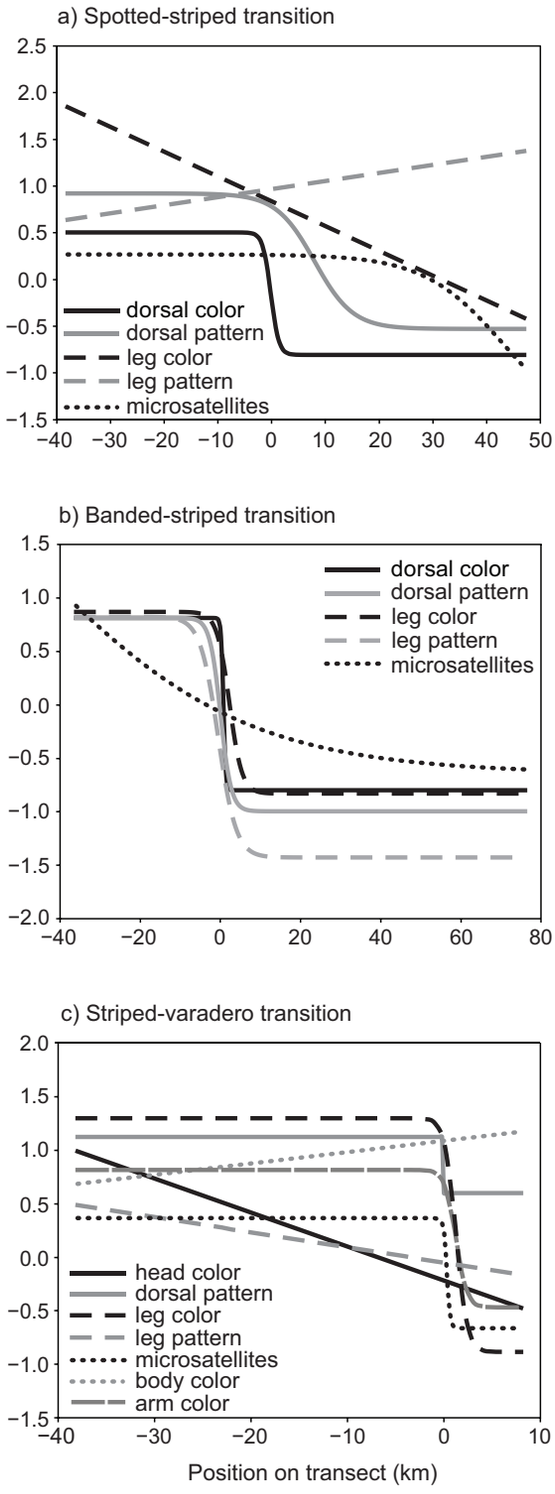

Figure 2: Cline comparison between three mimetic transition zones in *Ranitomeya imitator*: *a*, spotted-striped transition zone; *b*, banded-striped transition zone, and *c*, striped-varadero transition zone. Data from transition zone *c* are adapted from Twomey et al. (2014*a*; data available at Dryad Data Repository, http://dx.doi.org/10.5061/dryad.rd586; Twomey et al. 2014*b*). In all panels, clines are plotted along the sampling transect (*X*-axis, in km). Color pattern metrics were derived from a kernel discriminant analysis; the *Y*-axis thus represents discriminant scores (except for microsatellite clines; see below). For the spotted-striped transition (*a*), values closer to +1 indicate closer similarity to highland *Ranitomeya variabilis* and those closer to −1 similarity to lowland *R. variabilis*. For the banded-striped transition (*b*), values closer to +1 indicate closer similarity to *R. summersi* and those closer to −1 similarity to lowland *R. variabilis*. For the striped-varadero transition (*c*), values closer to +1 indicate closer similarity to lowland *R. variabilis* and those closer to −1 similarity to *Ranitomeya fantastica*. For the microsatellite clines, the *Y*-axis is defined as the first axis from a factorial-correspondence analysis. For all panels, the clines represent the best-fit lines from the best-supported model according to the Akaike information criterion corrected for small sample size.

to the striped morph, we found a rapid shift in dorsal color (orange to yellow), dorsal pattern (stripes running across body to stripes running along body), leg color (orange to blue), and leg pattern (stripes running along the leg to a reticulated pattern; figs. 2, A4*a*). These shifts occurred over a narrow geographic zone near Chipesa, Callanayacu, and Ricardo Palma. With the exception of leg color, all color pattern metrics had a center parameter estimate close to 0 (table A6), indicating that the statistically inferred center of the transition zone occurred close to our initial estimate of the transition zone center. The leg color cline, however, appeared to be shifted 1.5–3 km into the striped-morph side of the transition zone, and the 95% confidence interval for the center parameter does not include 0 (table A6). There was variation in the widths of the color pattern clines, ranging from narrow (1.16 km for dorsal color) to relatively wide (8.97 km for leg pattern).

We can inspect the mutual-information (MI) plots (fig. A1) to determine the contribution of the original color pattern variables to the respective discriminant scores. This reveals which specific aspects of the color pattern shift along the transect. For dorsal color, the highest MI with the discriminant-function metric was for body hue (H body), followed by brightness in the red-green range of the head (LM head), head chroma (i.e., color purity; C head), and head hue (H head). For leg color, all variables except leg brightness (Qt legs) showed high MI with the leg color metric. On the basis of these results, aspects of color (hue, in particular) contributed substantially to both the dorsal-color and leg color metrics, whereas brightness contributed relatively little. For dorsal pattern, all variables except color/noncolor ratios (c3bwratio and c4bwratio) and gradient orientation histograms where the extraction parameter *b* was equal to 0 showed high MI with the dorsal-pattern discriminant metric. For leg pattern, several metrics showed moderately high MI, with many of the gradient orientation histograms showing higher MI, on average, than the shape index histograms.

The factorial-correspondence analysis (FCA) on the microsatellite data generated four main axes, which together accounted for 54.1% of the genetic variation. Most of this was captured by axes 1 and 2, which accounted for 20.6% and 16.8% of the genetic variation, respectively. For the cline analyses, we analyzed only the first major axis from the FCA. We did, however, visually inspect FCA axes 2–4 and found that they showed no clear trend across the transect. Our cline analysis of FCA axis 1 showed that the data were best explained by a sigmoidal model of variation along the transect (table A6; fig. A4*a*). However, the point estimate for cline width was so wide (106.97 km) that the resulting model was effectively linear (fig. A4*a*). Furthermore, the center estimate for the microsatellite cline was highly discordant (−47.68 km) relative to center estimates from the color pattern metrics.

On the basis of our results from global regression, the best-supported model was one where all four color pattern metrics and microsatellite clines had unique center and width parameters. In other words, because parameters were constrained to be equal among different clines, there was always a substantial reduction in model fit. However, upon comparing AIC_c (Akaike information criterion corrected for small sample size) values, we see that all models where the microsatellite cline was constrained to have a common width or center with the color pattern clines resulted in substantially worse fits than models where the microsatellite cline was unconstrained (table A4). For example, in table A4, models b–d all involved constraining the microsatellite cline to share a parameter with the color pattern clines, whereas in models e–g the microsatellite cline was free to take on its own independent parameter values. We see that by relaxing the constraints on the microsatellite cline (models e–g), we obtained a much better model fit (average $AIC_c = -1{,}406.12$) than when microsatellites and color pattern metrics were constrained simultaneously (models b–d, average $AIC_c = -1{,}337.30$), corresponding to a ΔAIC_c of 68.82. From this, and the point estimates for cline parameters, we can conclude that the microsatellite cline has a shape and position very different from those of the color pattern clines and is effectively linear across the transect. Finally, we see that it is possible to constrain color pattern clines to have equal width with only a modest reduction in fit ($\Delta AIC_c = 5.86$; table A4, model f). Therefore, while the best-supported model may be one where each color pattern metric has a unique width, constraining the widths to be equal still gives a reasonable fit.

Color Pattern and Microsatellite Cline Analysis: Spotted-Striped Transect

For the spotted-striped transect, only dorsal color and dorsal pattern showed sigmoidal variation along the sampling transect, whereas leg color and leg pattern were best described by a linear model (figs. 2, A4*b*; table A7). These results fit with our observations made during field sampling, as there was a clear shift in dorsal color (green to yellow) and dorsal pattern (spotted to striped) between the two morphs, whereas the color and pattern of the legs showed no clear transition. The center estimate for dorsal color was close to 0 (−0.17 km); however, the center of the dorsal-pattern cline appeared to be shifted north toward the striped morph (center = 7.96 km). In addition, the width estimates between the dorsal color and dorsal pattern were distinct, with dorsal color showing a much narrower cline (2.94 km) than dorsal pattern (14.31 km). Therefore, our data suggest that, along the transect toward the striped morph, dorsal color shifts earlier and more abruptly than dorsal pattern. This discordance between color and pattern clines is exemplified at the sampling locality Upper Pongo 1 (km 1.44 on fig. A4*b*). We see that Upper Pongo 1 has a dorsal-color value typical of the striped morph (i.e., yellow); however, the dorsal pattern value is more typical of the spotted morph.

In the mutual-information (MI) plots (fig. A2) for the two variables showing sigmoidal variation, we see that variation in the red-green spectrum of the head (LM head) and body (LM body) and head hue (H head) all showed high MI with the dorsal-color metric. For dorsal pattern, most of the variables showing high MI were those extracted from the lower dorsum (prefix c3), whereas those extracted from the head (prefix c4) showed relatively low MI. Taking these results together, we can conclude that the clinal shift in color pattern is primarily due to hue variation on the dorsum and patterning variation on the lower dorsum.

The factorial-correspondence analysis (FCA) on the microsatellite data generated four main axes, which together described 77.5% of the genetic variation. Most of this variation was captured by axes 1 and 2, which accounted for 30.3% and 21.3% of the genetic variation, respectively. With respect to axis 1, two clusters are evident: Micaela Bastidas (allopatric striped; fig. 1, population H) and all other populations. With respect to axis 2, the Pinto Recodo population forms its own cluster (allopatric spotted; fig. 1, population A). These results are consistent with the Structure results (fig. 3*b*): when two populations were allowed, Micaela Bastidas was distinct from all other populations, and when three or more populations were allowed, Pinto Recodo was recovered as a distinct group. We performed clinal analyses on FCA axis 1 and found that the data best fit a sigmoidal model of variation along the transect (figs. 2*b*, A4*b*; table A7). However, the estimates for center (43.26 km) and width (29.93 km) were highly discordant relative to the color pattern clines and showed wide confidence intervals (table A7).

The global regression analysis shows that the best-supported model was one where each variable (dorsal color,

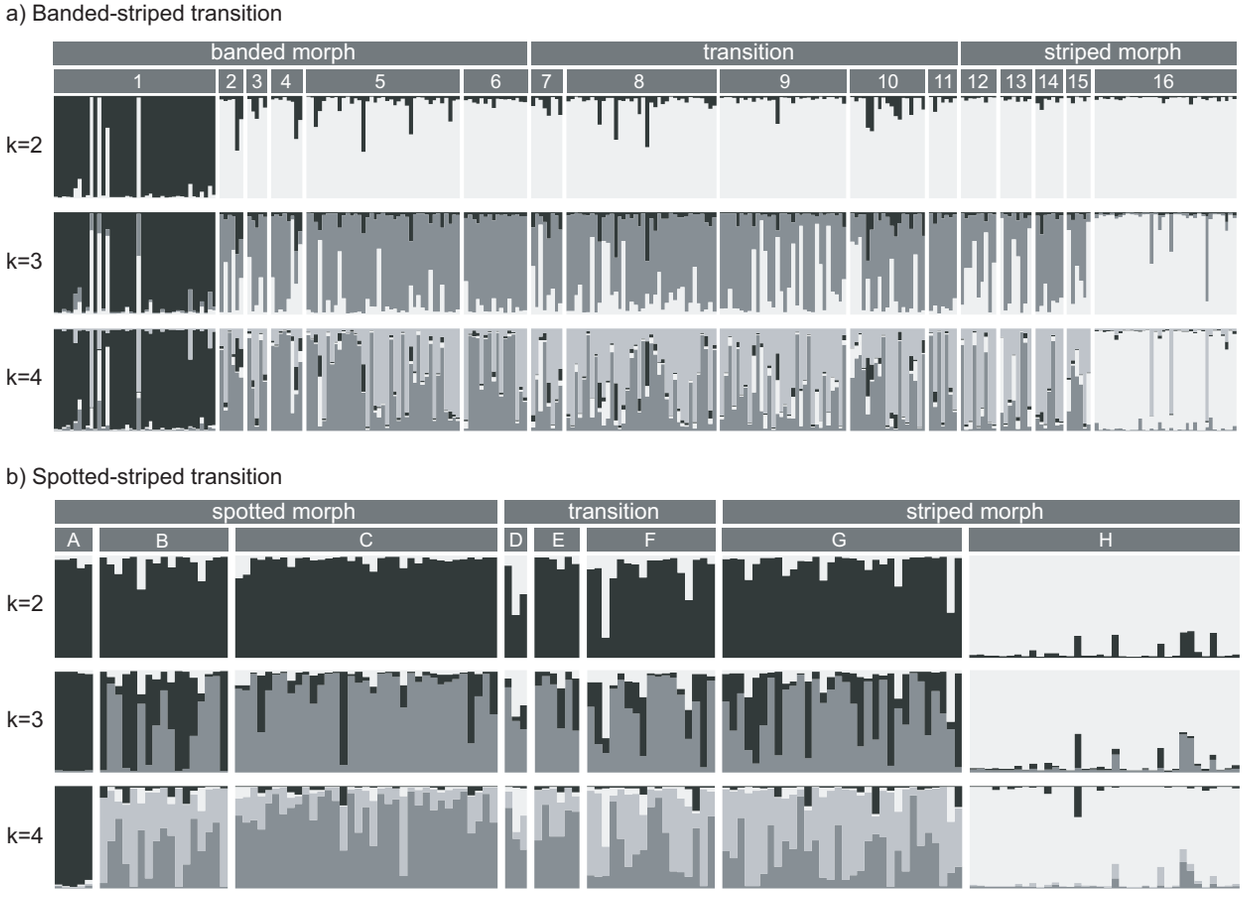

Figure 3: Structure plots based on microsatellite data for the banded-striped transition zone (*a*) and the spotted-striped transition zone (*b*). Vertical bars represent single individuals. Bar colors represent posterior probabilities of assignment to inferred genotypic group, where the number of groups (K) was allowed to vary from 2 to 4. For the banded-striped transition, the best-supported number of groups was $K = 3$; for the spotted-striped transition, the best-supported $K = 2$. Horizontal bars indicate mimetic morph (upper) and sampling locality (lower). Sampling locality codes correspond to tables A1 and A2 and figure A1, available online.

dorsal pattern, and microsatellite FCA axis 1) has unique center and width parameters. However, by inspecting the AIC_c values of each model, we found that constraining the microsatellite cline along with the color pattern clines (table A5, models b–d) greatly reduced model fit ($\Delta AIC_c = 74.0$), compared to models where microsatellite clines were unconstrained (table A5, models e–g). Also, constraining either center or width to be equal among the color pattern clines substantially reduced model fit (ΔAIC_c when centers were constrained $= 19.83$, ΔAIC_c when widths were constrained $= 15.27$), indicating that the clines for these two metrics have distinct shapes and positions.

Landscape Genetics

For the banded-striped transect, the best-supported number of populations in the Structure analysis was $K = 3$ (Delta K peak $= 41.1$). These three populations are Sauce (banded morph, population 1 in fig. 3*a*), Micaela Bastidas (striped morph, population 16 in fig. 3*a*), and a phenotypically heterogeneous central Huallaga group (populations 2–15 in fig. 3*a*). Most of the genetic structure appears to be associated with geographic distance. For example, Sauce is on the southern end of the transect and separated from the nearest sampling locality (Vaquero) by a mountain range rising to approximately 1200 m elevation (for comparison, the highest recorded elevation for *Ranitomeya imitator* is 945 m). Similarly, Micaela Bastidas is on the northern end of the transect, roughly 60 km from the nearest sampling locality. Therefore, the genetic distinctness of these two populations is likely due to isolation by distance. The central Huallaga group spans the banded-striped transition zone, yet there is no discernible genetic structure across the phenotypic transition (fig. 3*a*). Using multiple-matrix regression

(Wang 2013), we determined that the geographic distance between populations was significantly correlated with genetic distance ($\beta_D = 0.752, P = .0018$), whereas color pattern distance was not ($\beta_{CP} = 0.037, P = .421$). These results support an isolation-by-distance model of genetic divergence among populations and provide quantitative support for the interpretation of the Structure analysis.

For the spotted-striped transect, the best-supported number of populations in the Structure analysis was $K = 2$ (Delta K peak = 329.1). The two populations correspond to Micaela Bastidas (striped morph, population H in fig. 3*b*) and a larger group containing populations A–G (fig. 3*b*). This latter group is distributed in the Cordillera Escalera mountains and surrounding lowlands and includes pure spotted populations (e.g., San Jose, population C) and pure striped populations (e.g., Pongo, population G). Increasing the values of K to 3 or 4 revealed additional structure, in that the Pinto Recodo population was distinct; however, we did not find any genetic structure across the phenotypic-transition zone. Again, genetic structure was associated with geographic isolation, as the geographically distant populations Micaela Bastidas and Pinto Recodo were distinct. The multiple-matrix regression analysis revealed a marginally significant correlation between geographic distance and genetic distance ($\beta_D = 0.678, P = .054$) but no correlation between color pattern distance and genetic distance ($\beta_{CP} = -0.317, P = 0.274$). These results provide marginal support for an isolation-by-distance model of genetic divergence among populations and reject the isolation-by-adaptation hypothesis.

Approximate Bayesian Computation

The six demographic scenarios with the highest posterior probabilities for each group are shown in figure A3. Most of these scenarios share certain similarities; for example, all six show relatively recent common ancestry between the striped and spotted morphs, and five of the six scenarios show that the earliest splitting events involve the banded and varadero populations (the exception being scenario 27). Of these six scenarios, scenario 3 had, by far, the highest posterior probability (pp; scenario 3 pp = 0.49 vs. pp = 0.07–0.16 for all others) when we used the logistic-regression comparison method. This scenario involves an initial split between the varadero and banded populations, with a later split between the striped and varadero populations and, finally, admixture between the striped, banded, and spotted populations. Although this would suggest that the divergence time between the varadero and striped populations (t_2; fig. A5) predates admixture between the striped, spotted, and banded populations (t_1; fig. A5), the 95% confidence intervals (CIs) for these two parameters broadly overlap (t_1 point estimate = 4,360 generations ago [95% CI = 881–11,200]; t_2 point estimate = 9,400 generations ago [95% CI = 2,020–19,000]).

Mate Choice: Banded-Striped

We had a total of 119 successful free-release trials across the four sampled populations (allopatric banded, $n = 35$; transition zone banded, $n = 22$; transition zone striped, $n = 24$; allopatric striped, $n = 38$). In total, we recorded 40.35 h of courtship time across all trials, with an average of 20.3 min of total courtship time per trial. Comparing allopatric banded and allopatric striped populations (fig. 4*a*), we found a significant effect of male origin on courtship time ($\chi^2 = 8.03, \text{df} = 1, P = .005$), indicating that courtship preferences were significantly different between these two populations. This is likely due to the allopatric banded population's preference for its own morph, as the allopatric striped population did not seem to show a preference toward either morph, whereas the allopatric banded population showed a significantly higher courtship time with its own morph (fig. 4*a*). We also found a significant effect of pair ID on courtship time ($\chi^2 = 8.65$, df = 1, $P = .003$), indicating that female identity influences courtship preferences exhibited by males. Comparing transition zone banded and transition zone striped populations (fig. 4*b*), we found no significant effect of male origin on courtship time ($\chi^2 = 3.32$, df = 1, $P = .069$). In addition, we found no significant effect of pair ID on courtship time ($\chi^2 = 1.86$, df = 1, $P = .173$).

For the plastic-model mate choice experiments, we had a total of 85 successful trials across the four sampled populations (allopatric banded, $n = 22$; transition zone banded, $n = 21$; transition zone striped, $n = 22$; allopatric striped, $n = 20$). We recorded a total of 18.39 h of interaction time (i.e., time on platform), with an average of 18.4 min of interaction time per trial. We found no significant effect of male morph on interaction time ($\chi^2 = 0.01$, df = 1, $P = .929$) and no significant effect of transect position on interaction time ($\chi^2 = 2.27$, df = 1, $P = .132$; fig. A6*a*). There was also no significant interaction between male morph and transect position with respect to interaction time ($\chi^2 = 0.46$, df = 1, $P = .495$; fig. A6*a*). For calls (fig. A6*b*), there were fewer (total $n = 56$) successful trials (allopatric banded, $n = 17$; transition zone banded, $n = 11$; transition zone striped, $n = 12$; allopatric striped, $n = 16$) because males interacted with plastic models but did not call in some trials. We recorded a total of 2,003 calls directed toward plastic models, with an average of 36 calls per trial. We found a significant effect of male morph on calling behavior ($\chi^2 = 5.43$, df = 1, $P = .0197$), with banded males directing more calls toward models with their own morphotype (fig. A6*b*). However, there was no significant effect of transect position ($\chi^2 = 0.192$, df = 1, $P = .661$). Finally, there was no significant interaction between the effects of male morph and

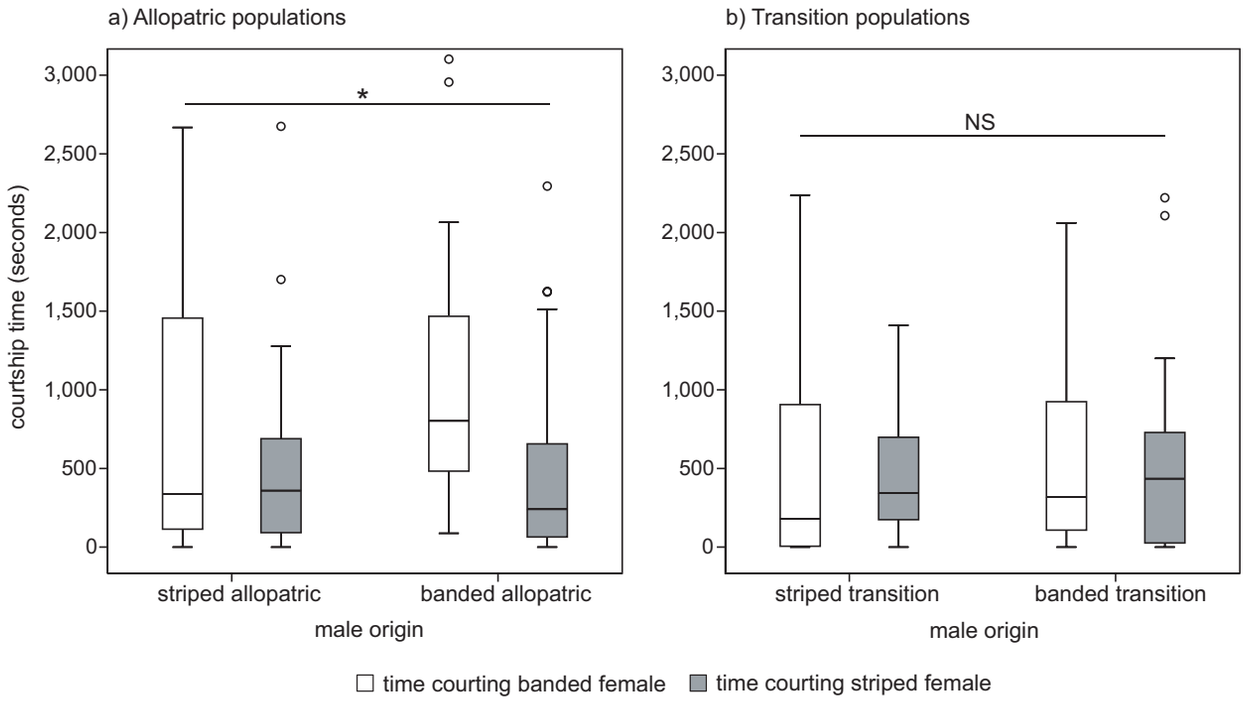

Figure 4: Box plots showing courtship times in the banded-striped free-release mate choice experiment. *a*, Allopatric-populations experiment, where banded and striped frogs originated from the ends of the sampling transect. *b*, Transition-populations experiment, where banded and striped frogs originated from near the mimetic transition zone. The asterisk indicates a statistically significant effect ($P < .05$) of male origin on courtship times from the generalized linear mixed model. Circles represent outliers. NS = not significant.

transect position with respect to calling behavior ($\chi^2 = 0.926$, df = 1, $P = .336$).

Mate Choice: Spotted-Striped

For the spotted-striped mate choice experiment, we had a total of 94 successful free-release trials across the three sampled populations (spotted, $n = 40$; transition zone striped, $n = 29$; allopatric striped, $n = 25$). We recorded a total of 34.92 h of courtship time across all trials, with an average of 22.3 min of total courtship time per trial. We found a marginally significant effect of male origin on courtship time ($\chi^2 = 4.93$, $P = .0852$) and a strong effect of pair ID on courtship time ($\chi^2 = 10.16$, $P = .0014$). The marginal effect of male origin may be due to the apparent preference by each striped population for its own morph (fig. 5). However, as the effect was not significant, we cannot conclude that mate preferences are different among populations tested in this experiment.

Discussion

Using quantitative analyses of color pattern in combination with cline analyses, we have demonstrated the existence of two narrow mimetic transition zones in the poison frog *Ranitomeya imitator*. The banded-striped transition zone is characterized by abrupt shifts in color and pattern on both the dorsum and the hindleg. The widths of these shifts varied substantially among different color pattern metrics. Dorsal color showed the narrowest cline width of 1.16 km, whereas leg pattern showed the widest cline width of 8.97 km. In the spotted-striped transition zone, the transition is characterized by an abrupt shift in dorsal color, a relatively gradual shift in dorsal pattern, and a smooth (linear) shift in both leg color and leg pattern. Dorsal color showed a relatively narrow cline 2.94 km wide, whereas the cline in dorsal pattern was much wider, at 14.31 km. One explanation for differences among cline widths on phenotypic traits is that the strength of selection differs across the traits (Haldane 1948; Endler 1977; Mallet et al. 1990). For a cline stabilized by positive frequency-dependent selection, the width of a cline can be expressed as $w = K\sigma/s^{1/2}$, where σ is dispersal distance, s is the selection coefficient, K is a constant (here we used $K = 12^{1/2}$, following Mallet and Barton 1989), and w is the width of a cline (Endler 1977). We can then calculate the strength of selection needed to produce a cline of the observed width, given our dispersal estimate (for *R. imitator*, 0.095 km/generation; see Twomey

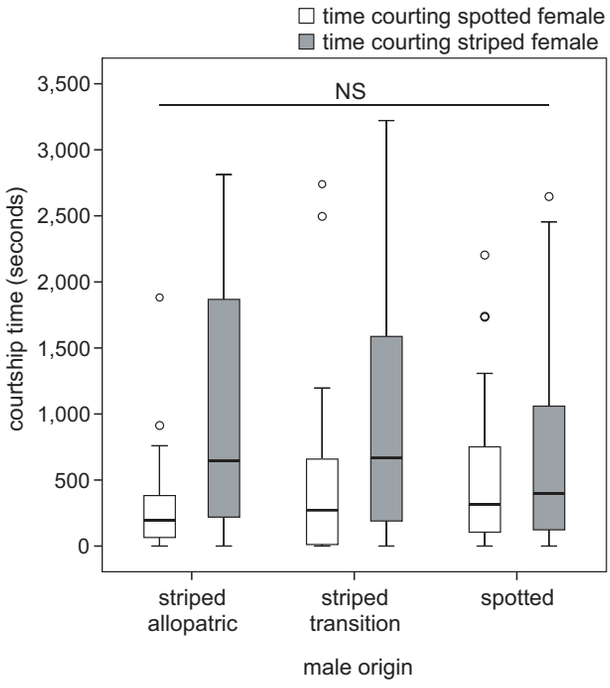

Figure 5: Box plot showing courtship times in the spotted-striped free-release mate choice experiment. The significance test is based on a generalized linear mixed model test for the effect of male origin on courtship time. Circles represent outliers. NS = not significant.

et al. 2014*a*). For the banded-striped transition zone, this gives a selection coefficient on dorsal color of 8.03%, compared to 0.13% for leg pattern. For the spotted-striped transition zone, dorsal color shows a narrower width (2.94 km) than dorsal pattern (14.31 km), giving selection coefficients on dorsal color and dorsal pattern of 1.25% and 0.05%, respectively. We caution that these estimates are highly contingent on the dispersal estimate for *R. imitator*, which has never been measured directly but only inferred via population genetic methods. For example, a two-fold increase in the dispersal estimate would increase the selection coefficient for dorsal color in the banded-striped zone to 32%. Also, there is substantial uncertainty surrounding width estimates for many of the color pattern metrics. Including the confidence intervals, the dorsal-color cline in the banded-striped transect could be as wide as 8.08 km, while the dorsal-pattern cline in the spotted-striped transect could be as wide as 30.38 km.

In both transition zones, we generally saw higher estimated selection coefficients for dorsal color than for dorsal pattern, indicating that color may be under stronger selection than pattern for mimicry. For leg color and pattern, we saw two distinct trends when comparing the two transition zones. In the banded-striped transition zone, both leg color and leg pattern followed a clear sigmoidal cline, whereas in the spotted-striped transition zone, leg color and pattern followed gradual, linear trends and were only subtly different among the spotted and striped morphs of *R. imitator*. This can probably be explained in terms of model-species variation, as the highland and lowland morphs of *Ranitomeya variabilis* have similar leg coloration (greenish-blue reticulation), whereas lowland *R. variabilis* and *Ranitomeya summersi* have distinct leg coloration (greenish-blue reticulation vs. orange bands). For the banded morph of *R. imitator*, it is perhaps surprising that the color pattern of the legs so clearly corresponds to that of *R. summersi*, given that the legs are a seemingly small component of the overall mimetic signal. The most likely explanation is that the legs are important for mimicry and thus subject to selection for mimetic resemblance. Indeed, leg color also seems to be important for mimicry in the striped-varadero transition zone, as does the color of the upper arms (Twomey et al. 2014*a*). An alternative possibility is that the color patterns of both the legs and the dorsum in the banded morph are controlled by the same set of genes or that the dorsal-banding genes are epistatic to the leg color genes.

Despite strong phenotypic differences across mimetic transition zones, we found no associated genetic structure across these zones. Rather, population genetic structure was always associated with allopatric populations rather than distinct phenotypes (fig. 3). This lack of mimicry-associated genetic structure was also confirmed by our landscape genetic analyses. For both transition zones we found that among-population genetic distance was correlated with geographic distance but not with color pattern distance (fig. A7), suggesting that color pattern divergence across these two transition zones has not resulted in a barrier to gene flow. These results stand in contrast to the results from the striped-varadero transition zone (Twomey et al. 2014*a*), where genetic divergence was correlated with both color pattern distance and geographic distance. In another dendrobatid species, *Oophaga pumilio*, Wang and Summers (2010) found that genetic divergence was primarily associated with divergence in dorsal coloration. One mechanism for morph-associated genetic isolation is "immigrant inviability," where immigrant individuals are at a selective disadvantage because of a phenotype-environment mismatch (Nosil et al. 2005). This could come about in two ways. First, because aposematic phenotypes are predicted to be under positive frequency-dependent selection, individuals with the wrong phenotype should experience higher predation risk. The possibility of immigrant inviability via increased predation has been supported by a number of studies in dendrobatids (Noonan and Comeault 2009; Chouteau and Angers 2011, 2012; Comeault and Noonan 2011; Willink et al. 2014), where reciprocal transplants of colored clay models have generally found higher attack rates on foreign than on local phenotypes. Second, im-

migrants may be at a mating disadvantage, as several studies in dendrobatids have found morph-based positive assortative mating (Summers et al. 1999; Reynolds and Fitzpatrick 2007; Maan and Cummings 2008; Richards-Zawacki and Cummings 2011; Richards-Zawacki et al. 2012; Twomey et al. 2014*a*). In the case of *R. imitator*, both transition zones studied here are substantially wider (roughly 3–6 km) than the species' estimated dispersal capabilities (0.095 km/generation), suggesting that for a given individual, dispersal across morph boundaries is not feasible. Rather, dispersal and gene flow between morphs most likely occur through the transition zone. Interestingly, in a clay-model study of the spotted-striped transition zone, Chouteau and Angers (2012) found that there was much lower predation overall (on any morph) in the transition zone sites than in the striped and spotted populations. This reduced predation pressure may facilitate the persistence of nonmimetic hybrids.

Our free-release mate choice experiments indicate that most of the populations studied here do not show any discernible preference for their own morph versus an alternate morph. However, there was one exception: the allopatric banded morph demonstrated a significant preference for its own morph. Furthermore, as this preference for banded frogs was not seen in the allopatric striped population, we can conclude that this preference is not due to banded females simply being more attractive (e.g., by virtue of their larger body size). However, we found no preferences in the transition zone populations, with both the transition zone banded and striped morphs showing random courtship with respect to morph type. This relaxed assortative mating at the transition zone is consistent with the population genetic results, which show a lack of genetic structure across morph boundaries. Similarly, for the spotted-striped transition zone, we found that none of the three populations tested showed a significant preference for either morph. There was a general trend for striped frogs to prefer their own morph (fig. 5), but this preference was not statistically significant. This is also consistent with the lack of genetic structure across the mimetic transition zone, which may be due to random mating with respect to morph.

As the free-release trials allowed frogs to make courtship decisions using all available cues (e.g., color pattern, acoustic, behavioral, olfactory), these trials provided an assessment of the premating isolation between two morphs when all potential cues were present. However, as these trials did not isolate the cues used in mate choice, we conducted additional mate choice experiments using plastic frog models to determine whether assortative mating was specifically based on color pattern. We found mixed results, depending on our choice of response variable. When measuring interaction time, we found no evidence for preferences in any population, but when measuring calling behavior, we found that banded males directed more calls toward banded models than toward striped models. Calling behavior is a more stringent response variable, in that a male could "interact" with a model without necessarily showing courtship interest. Interaction time was simply scored as time spent on the model's platform, with no information on male orientation or interest, whereas calling is a behavior specifically associated with courtship. On the basis of these results, color pattern may be one of the cues involved in mate choice in this system. Color pattern could represent a "magic trait," that is, a trait subject to divergent ecological selection that also mediates mate choice (Gavrilets 2004). Identifying such traits is of interest in speciation research, as they are thought to facilitate speciation with gene flow. In *Heliconius* butterflies, wing color pattern represents a good example of a magic trait (Jiggins et al. 2001; Merrill et al. 2012). Selection for Müllerian mimicry has caused wing color patterns to diverge as different populations participate in distinct mimicry rings, and there is substantial evidence that wing color pattern itself mediates assortative mating (Jiggins et al. 2001, 2004). However, even if color pattern alone does contribute to assortative mating in the banded-striped transition zone of *R. imitator*, the absence of assortative mating in the free-release trials (where all cues are present) indicates that color pattern differences may not impede gene flow where the two distinct morphs come into contact.

In a previous study on the striped-varadero transition zone (Twomey et al. 2014*a*), color pattern clines were narrower (approx. 1–4 km; fig. 2), there was strong genetic structuring between morphs at the transition zone, and the striped morph from the transition zone displayed a significant mating preference for its own morph (table 1). Thus, in the striped-varadero transition zone, it appears that mimetic divergence has led to a breakdown in gene flow between morphs, which may represent incipient ecological speciation. In the two transition zones studied here, mimetic divergence has caused varying levels of phenotypic differentiation but has not slowed gene flow between morphs. Thus, the *R. imitator* mimicry system is useful for comparative analyses of the factors influencing progress toward speciation, given that we observe three transition zones at seemingly different stages of divergence (table 1; fig. 2). Furthermore, as these mimetic populations are all members of the same species, we can identify isolating barriers that arise in the early stages of population divergence.

Differential Progress along the Speciation Continuum

Overall, these results strongly suggest the existence of a "speciation continuum" among mimetic morphs of *R. imitator*, which we have now characterized at the geographic, phenotypic, behavioral, and genetic levels (table 1). In the earliest stages of population divergence, here characterized

Table 1: Transition zone comparison

Transition zone	Transect length (km)	Elevation gradient?	Color pattern clines	Color pattern cline width (range; km)[a]	Genetic structure	Assortative mating	Model species
Spotted-striped	83	Yes	Sigmoidal shift in dorsal color and dorsal pattern; centers offset by approximately 8 km	2.95 (2.93–14.31)	Isolation by distance; no structure across mimetic transition zone	Weak or absent; no significant effect of color pattern or location of origin in mate choice	Single polytypic model species; *Ranitomeya variabilis* is polytypic along an elevational gradient; this variation is tracked by *Ranitomeya imitator*
Banded-striped	106	No	Sigmoidal shift in dorsal color, dorsal pattern, leg color, and leg pattern; centers nearly coincident	5.35 (1.20–8.97)	Isolation by distance; no structure across mimetic transition zone	Weak, color pattern based; associated with allopatric populations and male call preference in plastic-model study	Model species parapatric; mimetic shift in *R. imitator* coincides with parapatry between *Ranitomeya summersi* and *R. variabilis*
Striped-varadero[b]	39	No	Sigmoidal shift in arm color, leg color, and body pattern; cline centers are statistically coincident	1.45 (.1–4.15)	Isolation by adaptation and isolation by distance; structure coincides with mimetic transition zone	Moderate, asymmetrical; striped frogs from transition zone prefer own morph	Model species overlap; both model species (*Ranitomeya fantastica* and *R. variabilis*) present on both sides of the mimetic transition zone

[a] Cline width estimates represent the point estimate for the color pattern clines when widths were constrained to be equal. Ranges in cline width represent the range of point estimates for each color pattern clines.
[b] Data from Twomey et al. (2014*a*).

by the spotted-striped transition zone, there is divergence in mimetic color pattern but little else. Phenotypic clines are seen in only two aspects of the color pattern; these clines are relatively wide and do not show geographical coincidence. In the next stage, here characterized by the banded-striped transition zone, there are clines in several aspects of the color pattern; these clines are generally narrower and roughly geographically coincident. Mating preferences are apparent, but only in allopatric populations: transition populations show no preferences, and gene flow among morphs is unimpeded. Finally, in the later stage, here characterized by the striped-varadero transition zone, clines are very narrow, apparent in several aspects of the mimetic color pattern, and geographically coincident. Mating preferences exist at the transition zone, and gene flow is restricted. In addition, there is divergence in other traits (body size, advertisement calls) that have clines geographically coincident with the color pattern clines.

Given the wide range of examples highlighting the variation in completeness of ecological speciation (see Nosil et al. 2009 for a review), a key goal of speciation research to understand the reasons for this variation. Factors influencing progress toward speciation generally fall into two classes: nonselective and selective (Nosil et al. 2009; Nosil 2012). Here, we discuss three nonselective factors (divergence time, geographic barriers, and secondary contact) and two selective factors ("stronger selection" and "multifarious selection") to understand differential progress toward speciation in *R. imitator*.

First, the amount of reproductive isolation between two populations should increase with divergence time (Coyne and Orr 1989; Sasa et al. 1998). Our results from the ABC analysis suggest that divergence times between the four mimetic morphs of *R. imitator* only partially explain variation in reproductive isolation. The best-supported demographic scenario (fig. A5) indicates recent admixture between the striped, spotted, and banded morphs (approx. 4,000 generations ago), with a somewhat older divergence time between the varadero morph and other populations (approx. 9,400 generations ago). However, confidence intervals on these divergence-time estimates overlap widely, and the branching order of these four populations is somewhat ambiguous (fig. A3). Furthermore, pairwise genetic distances (Nei's *D*) are higher between the banded and striped populations (1.148) than between the varadero and striped populations (0.492) or between the spotted and striped populations (0.538). Overall, these results suggest that the divergence time between the varadero and striped populations is approximately equal to, or perhaps slightly older than, the divergence time between the banded and striped populations and that between the spotted and striped populations.

Second, geographic isolation may facilitate ecological speciation when geographic barriers occur between ecomorphs. Populations that are divergent ecologically and also separated by some geographical barrier should diverge more readily than those where that geographic barrier is absent, as in the latter case divergent selection is no longer counteracted by gene flow (Nosil 2012). This may be particularly relevant for clines stabilized by positive frequency-dependent selection, which can form in seemingly arbitrary geographic areas but can shift position over time and may eventually become "trapped" at geographical barriers (Bazykin 1969; Mallet 1986; Mallet and Barton 1989; Blum 2002). In *R. imitator*, we might therefore expect to see geographic barriers separating mimetic morphs, especially at Varadero, where isolation is strongest. However, this is not what we observe, as the transition zone at Varadero occurs across approximately 1–2 km of unimpeded lowland rainforest habitat. While there is a small river nearby, this river is roughly 1 km south of the transition zone, and striped populations on either side of the river are not genetically isolated (Twomey et al. 2014*a*). In the banded-striped transition zone, the much larger Huallaga River also does not appear to be an important barrier. For example, in figure 3*a*, populations 6–7, 9–10, 11–12, and 14–15 are on opposite sides of the Huallaga River. However, farther upstream (outside the transition zone), this river may be a barrier between the spotted and banded populations, as we have found pure spotted and pure banded morphs occurring on north and south sides of the river, respectively. We have not found intermediates between the banded and spotted morphs, which may suggest that these two morphs are somewhat isolated.

Third, historical allopatry between ecomorphs may also promote speciation (Rundle and Nosil 2005). In this view, previously isolated populations with subsequent secondary contact should exhibit greater reproductive isolation than populations that were isolated for a shorter time or were never isolated at all. As isolated populations are no longer subject to the homogenizing effects of gene flow, over time these populations may diverge in seemingly arbitrary characters. Thus, a signature of secondary contact between populations is congruent clines in many characters, not just those subject to divergent ecological selection (Coyne and Orr 2004). The striped-varadero transition zone is unique in that, in addition to clines in color pattern elements, there are congruent clines in advertisement calls, body size, and microsatellites (Twomey et al. 2014*a*). Compared to the two other transition zones, the striped-varadero zone is therefore the most suggestive of secondary contact. However, distinguishing whether hybrid zones are due to primary divergence or secondary contact is difficult (Barton and Hewitt 1985), and late-stage primary transition zones could show clines at neutral loci (and presumably neutral traits), provided that divergent selection is strong enough to pose a barrier to gene flow (Feder and Nosil 2010). In terms of biogeographical ev-

idence, there is nothing to suggest any historical isolation at the striped-varadero transition zone, as there are no major rivers or mountains in the area. Thus, whether the striped-varadero transition zone is a result of primary divergence or secondary contact remains unknown. Overall, genomic studies could be useful to better understand demographic influences (e.g., divergence times, bottlenecks, historical allopatry) on variation in reproductive isolation in this system.

We focus on two selective hypotheses explaining progress toward speciation. The "stronger-selection" hypothesis predicts that speciation is facilitated by strong selection on a single trait, whereas the "multifarious-selection" hypothesis predicts that speciation is facilitated by divergent selection on multiple independent traits (Nosil et al. 2009; Nosil and Harmon 2009). In the latter case, the total strength of divergent selection should be higher when adaptation occurs along multiple independent niche axes, in which case multifarious selection more readily drives speciation by increasing the total strength of selection (Nosil and Harmon 2009). Assuming a constant strength of selection, multifarious divergence may drive widespread genomic divergence as multiple loci are "pulled apart" by divergent selection, whereas strong selection on a single trait increases per-trait selection coefficients, facilitating divergence with gene flow (Mallet 2006). The "stronger-selection" hypothesis has received support in studies finding positive correlations between reproductive isolation and divergence in one phenotypic trait, for example, body size (McKinnon et al. 2004; Funk et al. 2006) or color pattern (Jiggins et al. 2004; Maan and Cummings 2008). In the context of our study, the "stronger-selection" hypothesis generates a clear prediction, which is that the magnitude of mimetic divergence will be positively correlated to levels of reproductive isolation. We can use the difference between the y_{max} and y_{min} parameters from our clinal analyses of color pattern to obtain an overall magnitude of mimetic shift across each transition zone. The difference between these parameters represents the overall cline height and therefore can be thought of as a mimicry effect size. If we do so, the banded-striped transition zone has the largest magnitude of mimetic divergence, 1.80, followed by the spotted-striped transition zone (1.35) and the striped-varadero transition zone (0.45). Thus, under the "stronger-selection" hypothesis, we would predict the banded-striped and spotted-striped transition zones to be the most reproductively isolated and the striped-varadero transition zone to be the least reproductive isolated, which is opposite from our observations. It is important to point out that this assumes that mimetic color pattern is effectively a single trait, which may not be the case. If different components of the mimetic color pattern are under independent genetic control, they may be better thought of as several different traits all undergoing divergent selection. Under the "multifarious-selection" hypothesis, we would therefore predict that reproductive isolation should be positively correlated with the number of color pattern traits under divergent selection. If we treat each color pattern metric as an independent trait, then in the spotted-striped transition zone divergent selection is acting on two traits (dorsal color and dorsal pattern), in the striped-varadero transition zone on three traits (arm color, leg color, and body pattern), and in the banded-striped transition zone on four traits (dorsal color, dorsal pattern, leg color, and leg pattern). From this, we would predict the banded-striped transition zone to show the strongest reproductive isolation, which is again not what we observed. However, as we do not know how many independent genetic loci are involved in the color pattern shift at each transition zone, we do not know whether the shifts should be treated as one or many axes of divergence.

One observation related to multifarious selection is that there is evidence of a shift in body size at the striped-varadero transition zone (Twomey et al. 2014*a*), while the other two transition zones show no such shift (fig. A8). Thus, at the striped-varadero transition zone, divergent selection may be acting on both mimetic color pattern and body size, versus color pattern only at the banded-striped and spotted-striped transition zones. Divergence in body size is frequently implicated in the evolution of reproductive isolation (McKinnon et al. 2004; Bolnick et al. 2006; Funk et al. 2006), and thus the observed reproductive isolation at the striped-varadero transition zone may have arisen from the combined effects of divergence in both mimicry and body size. While we do not yet understand the adaptive significance (if any) of the body-size shift at the striped-varadero transition, there are several intriguing possibilities that warrant further research. First, Twomey et al. (2014*a*) suggested that body size could be related to mimicry, as *Ranitomeya fantastica* (the model species of the larger varadero morph of *R. imitator*) is somewhat larger than *R. variabilis* (the model species of the smaller striped morph). Another possibility is that size represents an adaptation to distinct habitat types present in this area, although this would be independent of any shift in elevation, as only the spotted-striped transition occurs along an elevation gradient. During our fieldwork in the Varadero region, we mostly found the smaller striped morph in disturbed habitats, while the larger varadero morph was mostly found in undisturbed primary rain forest. While this could be a coincidence (given that the striped morph occurs in closer proximity to a human settlement), there are at least two ecological explanations for a habitat-related shift in body size. First, if disturbed habitats contain a poorer available diet relative to undisturbed habitats, the body-size shift may represent a plastic developmental response due to nutritional differences between the two habitats. Second, as *R. imitator* uses small phytotelmata (water bodies formed in plants) for reproduction, if breeding plant communities differ between the two habitats such that smaller plants (and phy-

totelmata) are found in the disturbed habitat while larger plants are found in the undisturbed habitat, body size could represent an adaptation for using smaller versus larger phytotelmata. While we do not have data on phytotelm size across the striped-varadero transition, it appears that smaller phytotelmata (e.g., *Calathea* spp.) predominate on the striped side of the cline while larger phytotelmata (e.g., *Heliconia* spp.) seem to be more common on the varadero side of the cline.

It is still unknown to what extent, if any, body size differences are responsible for reproductive isolation. While we have provided evidence that color pattern alone may be an important cue used in mate choice in the banded-striped transition zone, it is unknown whether the isolation seen at Varadero is due to differences in color pattern, body size, or a combination of the two. We note that the population that shows the mating preference (striped transition) is actually the smaller morph (fig. A8*c*); therefore, if preference were based on body size, it would have to be a preference shown by the striped morph for smaller-sized frogs. Future studies on the striped-varadero transition should investigate whether body size is an adaptive trait subject to divergent selection and whether color pattern and/or body size is a cue that mediate assortative mating.

Given these results, we can conclude that the striped-varadero transition zone is unique in at least two ways: (1) it is the only transition zone with evidence of assortative mating at the interface between distinct morphs, and (2) it is the only transition zone showing a shift in a trait possibly unrelated to mimicry (body size). The latter result lends support to the "multifarious-selection" hypothesis, which stipulates that ecological speciation is facilitated when divergent selection acts on multiple independent traits. Further, our results suggest that while color pattern diverges repeatedly, genome-wide divergence occurs only when there is assortative mating at a transition zone as well as divergence in multiple independent traits (e.g., body size, advertisement calls). These results underscore the importance of assortative mating as an early-evolving barrier that may be important in the early stages of population divergence.

Acknowledgments

We thank A. B. L. Larsen for discussion on image texture quantification, M. Kain for help with multiple-matrix regression, and J. Touchon for help with generalized linear mixed models. We thank J. Brown, S. Chen, M. Guerra-Panaifo, V. Holmes, T. Kosch, C. Lopez, M. Mayer, M. Pepper, R. M. Pezo, M. Sanchez-Rodriguez, L. Schulte, A. Stuckert, J. Tumulty, and J. Yeager for help in the field. This research was funded by a National Science Foundation doctoral dissertation improvement grant (1210313) awarded to E.T. and K.S., a National Geographic Society grant awarded to K.S. (8751–10), and a North Carolina Center for Biodiversity scholarship (2012) at East Carolina University awarded to E.T. Research permits were obtained from the Ministry of Natural Resources (DGFFS) in Lima, Peru (authorizations 050–2006-INRENA-IFFS-DCB, 067–2007-INRENA-IFFS-DCB, and 005–2008-INRENA-IFFS-DCB). Tissue exports were authorized under Contrato de Acceso Marco a Recursos Geneticos 0009–2013-MINAGRI-DGFFS/DGEFFS, with CITES (Convention on International Trade in Endangered Species of Wild Fauna and Flora) permit number 003302. All research followed an animal-use protocol approved by the Animal Care and Use Committee of East Carolina University.

Literature Cited

Barton, N. H., and G. Hewitt. 1985. Analysis of hybrid zones. Annual Review of Ecology and Systematics 16:113–148.

Bazykin, A. 1969. Hypothetical mechanism of speciation. Evolution 23:685–687.

Belkhir, K., P. Borsa, L. Chikhi, N. Raufaste, and F. Bonhomme. 1996. GENETIX 4.05, logiciel sous Windows TM pour la génétique des populations. Laboratoire génome, populations, interactions, Centre National de la Recherche Scientifique Unité Mixte de Recherche 5000, Montpellier, France.

Berner, D., A.-C. Grandchamp, and A. P. Hendry. 2009. Variable progress toward ecological speciation in parapatry: stickleback across eight lake-stream transitions. Evolution 63:1740–1753.

Blum, M. J. 2002. Rapid movement of a *Heliconius* hybrid zone: evidence for phase III of Wright's shifting balance theory? Evolution 56:1992–1998.

Bolnick, D. I., T. J. Near, and P. C. Wainwright. 2006. Body size divergence promotes post-zygotic reproductive isolation in centrarchids. Evolutionary Ecology Research 8:903–913.

Brown, J. L., M. Chouteau, T. Glenn, and K. Summers. 2009. The development and analysis of twenty-one microsatellite loci for three species of Amazonian poison frogs. Conservation Genetics Resources 1:149–151.

Brown, J. L., E. Twomey, V. Morales, and K. Summers. 2008*a*. Phytotelm size in relation to parental care and mating strategies in two species of Peruvian poison frogs. Behaviour 145:1139–1165.

Chamberlain, N. L., R. I. Hill, D. D. Kapan, L. E. Gilbert, and M. R. Kronforst. 2009. Polymorphic butterfly reveals the missing link in ecological speciation. Science 326:847–850.

Chouteau, M., and B. Angers. 2011. The role of predators in maintaining the geographic organization of aposematic signals. American Naturalist 178:810–817.

———. 2012. Wright's shifting balance theory and the diversification of aposematic signals. PLoS ONE 7:e34028. doi:10.1371/journal.pone.0034028.

Comeault, A., and B. Noonan. 2011. Spatial variation in the fitness of divergent aposematic phenotypes of the poison frog, *Dendrobates tinctorius*. Journal of Evolutionary Biology 24:1374–1379.

Cornuet, J.-M., P. Pudlo, J. Veyssier, A. Dehne-Garcia, M. Gautier, R. Leblois, J.-M. Marin, and A. Estoup. 2014. DIYABC v2.0: a software to make approximate Bayesian computation inferences about population history using single nucleotide polymorphism, DNA sequence and microsatellite data. Bioinformatics 30:1187–1189.

Cornuet, J.-M., F. Santos, M. A. Beaumont, C. P. Robert, J.-M. Marin, D. J. Balding, T. Guillemaud, and A. Estoup. 2008. Inferring population history with *DIY ABC*: a user-friendly approach to approximate Bayesian computation. Bioinformatics 24:2713–2719.

Coyne, J. A., and H. A. Orr. 1989. Patterns of speciation in *Drosophila*. Evolution 43:362–381.

———. 2004. Speciation. Sinauer, Sunderland, MA.

Dalal, N., and B. Triggs. 2005. Histograms of oriented gradients for human detection. Pages 886–893 *in* C. Schmid, S. Soatto, and C. Tomasi, eds. Proceedings, IEEE Computer Society Conference on Computer Vision and Pattern Recognition: CVPR 2005. Vol. 1. IEEE Computer Society, Los Alamitos, CA.

Earl, D. A., and B. M. vonHoldt. 2012. STRUCTURE HARVESTER: a website and program for visualizing STRUCTURE output and implementing the Evanno method. Conservation Genetics Resources 4:359–361.

Endler, J. A. 1977. Geographic variation, speciation, and clines. Princeton University Press, Princeton, NJ.

———. 1990. On the measurement and classification of colour in studies of animal colour patterns. Biological Journal of the Linnean Society 41:315–352.

Endler, J. A., and J. J. D. Greenwood. 1988. Frequency-dependent predation, crypsis and aposematic coloration. Philosophical Transactions of the Royal Society B: Biological Sciences 319:505–523.

Evanno, G., S. Regnaut, and J. Goudet. 2005. Detecting the number of clusters of individuals using the software STRUCTURE: a simulation study. Molecular Ecology 14:2611–2620.

Feder, J. L., and P. Nosil. 2010. The efficacy of divergence hitchhiking in generating genomic islands during ecological speciation. Evolution 64:1729–1747.

Funk, D. J., P. Nosil, and W. J. Etges. 2006. Ecological divergence exhibits consistently positive associations with reproductive isolation across disparate taxa. Proceedings of the National Academy of Sciences of the USA 103:3209–3213.

Gavrilets, S. 2004. Fitness landscapes and the origin of species. Princeton University Press, Princeton, NJ.

Gomez, D. 2006. AVICOL, a program to analyse spectrometric data. Updated October 2, 2013. http://sites.google.com/site/avicolprogram/.

Greenwood, J. J., P. A. Cotton, and D. M. Wilson. 1989. Frequency-dependent selection on aposematic prey: some experiments. Biological Journal of the Linnean Society 36:213–226.

Haldane, J. 1948. The theory of a cline. Journal of Genetics 48:277–284.

Hatfield, T., and D. Schluter. 1999. Ecological speciation in sticklebacks: environment-dependent hybrid fitness. Evolution 53:866–873.

Hendry, A., D. Bolnick, D. Berner, and C. Peichel. 2009. Along the speciation continuum in sticklebacks. Journal of Fish Biology 75:2000–2036.

Jiggins, C. D. 2008. Ecological speciation in mimetic butterflies. BioScience 58:541–548.

Jiggins, C. D., C. Estrada, and A. Rodrigues. 2004. Mimicry and the evolution of premating isolation in *Heliconius melpomene* Linnaeus. Journal of Evolutionary Biology 17:680–691.

Jiggins, C. D., R. E. Naisbit, R. L. Coe, and J. Mallet. 2001. Reproductive isolation caused by colour pattern mimicry. Nature 411:302–305.

Joron, M., and J. L. Mallet. 1998. Diversity in mimicry: paradox or paradigm? Trends in Ecology and Evolution 13:461–466.

Koenderink, J. J., and A. J. van Doorn. 1992. Surface shape and curvature scales. Image and vision computing 10:557–564.

Larsen, A. B., J. S. Vestergaard, and R. Larsen. 2014. HEp-2 cell classification using shape index histograms with donut-shaped spatial pooling. IEEE Transactions on Medical Imaging 33:1573–1580.

Lindeberg, T. 1996. Scale-space: a framework for handling image structures at multiple scales. Pages 27–38 *in* C. E. Vandoni, ed. CERN School of Computing: Egmond aan Zee, Netherlands, 8 September–21 September 1996: proceedings. CERN (European Organization for Nuclear Research), Geneva.

Maan, M. E., and M. E. Cummings. 2008. Female preferences for aposematic signal components in a polymorphic poison frog. Evolution 62:2334–2345.

Mallet, J. 1986. Hybrid zones of *Heliconius* butterflies in Panama and the stability and movement of warning colour clines. Heredity 56:191–202.

———. 2006. What does *Drosophila* genetics tell us about speciation? Trends in Ecology and Evolution 21:386–393.

Mallet, J., and N. Barton. 1989. Inference from clines stabilized by frequency-dependent selection. Genetics 122:967–976.

Mallet, J., N. Barton, G. Lamas, J. Santisteban, M. Muedas, and H. Eeley. 1990. Estimates of selection and gene flow from measures of cline width and linkage disequilibrium in *Heliconius* hybrid zones. Genetics 124:921–936.

Mallet, J., M. Beltrán, W. Neukirchen, and M. Linares. 2007. Natural hybridization in heliconiine butterflies: the species boundary as a continuum. BMC Evolutionary Biology 7:28. doi: 10.1186/1471-2148-7-28.

McKinnon, J. S., S. Mori, B. K. Blackman, L. David, D. M. Kingsley, L. Jamieson, J. Chou, and D. Schluter. 2004. Evidence for ecology's role in speciation. Nature 429:294–298.

Merrill, R. M., Z. Gompert, L. M. Dembeck, M. R. Kronforst, W. O. McMillan, and C. D. Jiggins. 2011. Mate preference across the speciation continuum in a clade of mimetic butterflies. Evolution 65:1489–1500.

Merrill, R. M., R. W. Wallbank, V. Bull, P. C. Salazar, J. Mallet, M. Stevens, and C. D. Jiggins. 2012. Disruptive ecological selection on a mating cue. Proceedings of the Royal Society B: Biological Sciences 279:4907–4913.

Mika, S., G. Rätsch, J. Weston, B. Schölkopf, and K. Müller. 1999. Fisher discriminant analysis with kernels. Pages 41–48 *in* Y.-H. Hu, J. Larsen, E. Wilson, and S. Douglas, eds. Neural networks for signal processing IX, 1999: proceedings of the 1999 IEEE Signal Processing Society workshop. Institute of Electrical and Electronics Engineers, New York.

Noonan, B. P., and A. A. Comeault. 2009. The role of predator selection on polymorphic aposematic poison frogs. Biology Letters 5:51–54.

Nosil, P. 2012. Ecological speciation. Oxford University Press, Oxford.

Nosil, P., B. Crespi, and C. Sandoval. 2003. Reproductive isolation driven by the combined effects of ecological adaptation and reinforcement. Proceedings of the Royal Society B: Biological Sciences 270:1911–1918.

Nosil, P., and L. Harmon. 2009. Niche dimensionality and ecological speciation. Pages 127–154 *in* R. Butlin, J. Bridle, and D. Schluter, eds. Speciation and patterns of diversity. Cambridge University Press, Cambridge.

Nosil, P., L. J. Harmon, and O. Seehausen. 2009. Ecological explanations for (incomplete) speciation. Trends in Ecology and Evolution 24:145–156.

Nosil, P., T. H. Vines, and D. J. Funk. 2005. Reproductive isolation caused by natural selection against immigrants from divergent habitats. Evolution 59:705–719.

Peakall, R., and P. E. Smouse. 2006. GENALEX 6: genetic analysis in Excel. Population genetic software for teaching and research. Molecular Ecology Notes 6:288–295.

Pritchard, J. K., M. Stephens, and P. Donnelly. 2000. Inference of population structure using multilocus genotype data. Genetics 155:945–959.

Puebla, O., E. Bermingham, F. Guichard, and E. Whiteman. 2007. Colour pattern as a single trait driving speciation in *Hypoplectrus* coral reef fishes? Proceedings of the Royal Society B: Biological Sciences 274:1265–1271.

R Development Core Team. 2005. R: a language and environment for statistical computing. R Foundation for Statistical Computing, Vienna.

Reynolds, R. G., and B. M. Fitzpatrick. 2007. Assortative mating in poison-dart frogs based on an ecologically important trait. Evolution 61:2253–2259.

Richards-Zawacki, C. L., and M. E. Cummings. 2011. Intraspecific reproductive character displacement in a polymorphic poison dart frog, *Dendrobates pumilio*. Evolution 65:259–267.

Richards-Zawacki, C. L., I. J. Wang, and K. Summers. 2012. Mate choice and the genetic basis for colour variation in a polymorphic dart frog: inferences from a wild pedigree. Molecular Ecology 21: 3879–3892.

Rosenblum, E. B. 2006. Convergent evolution and divergent selection: lizards at the White Sands ecotone. American Naturalist 167:1–15.

Rosenblum, E. B., and L. J. Harmon. 2011. "Same same but different": replicated ecological speciation at White Sands. Evolution 65:946–960.

Rundle, H. D., and P. Nosil. 2005. Ecological speciation. Ecology Letters 8:336–352.

Sasa, M. M., P. T. Chippindale, and N. A. Johnson. 1998. Patterns of postzygotic isolation in frogs. Evolution 52:1811–1820.

Schluter, D. 1996. Ecological speciation in postglacial fishes. Philosophical Transactions of the Royal Society B: Biological Sciences 351:807–814.

Seehausen, O. 2009. Progressive levels of trait divergence along a "speciation transect" in the Lake Victoria cichlid fish *Pundamilia*. Pages 155–176 *in* R. Butlin, J. Bridle, and D. Schluter, eds. Speciation and patterns of diversity. Cambridge University Press, Cambridge.

Seehausen, O., Y. Terai, I. S. Magalhaes, K. L. Carleton, H. D. Mrosso, R. Miyagi, I. van der Sluijs, et al. 2008. Speciation through sensory drive in cichlid fish. Nature 455:620–626.

Skaug, H., D. Fournier, A. Nielsen, A. Magnusson, and B. Bolker. 2011. glmmADMB: generalized linear mixed models using AD Model Builder. R package version 0.6 5:r143. http://glmmadmb.r-forge.r-project.org.

Stuckert, A. M., R. A. Saporito, P. J. Venegas, and K. Summers. 2014*a*. Alkaloid defenses of co-mimics in a putative Müllerian mimetic radiation. BMC Evolutionary Biology 14:76. doi: 10.1186/1471-2148-14-76.

Stuckert, A. M., P. J. Venegas, and K. Summers. 2014*b*. Experimental evidence for predator learning and Müllerian mimicry in Peruvian poison frogs (*Ranitomeya*, Dendrobatidae). Evolutionary Ecology 28:413–426.

Summers, K., R. Symula, M. Clough, and T. Cronin. 1999. Visual mate choice in poison frogs. Proceedings of the Royal Society B: Biological Sciences 266:2141–2145.

Symula, R., R. Schulte, and K. Summers. 2001. Molecular phylogenetic evidence for a mimetic radiation in Peruvian poison frogs supports a Müllerian mimicry hypothesis. Proceedings of the Royal Society B: Biological Sciences 268:2415–2421.

Szymura, J. M., and N. H. Barton. 1986. Genetic analysis of a hybrid zone between the fire-bellied toads, *Bombina bombina* and *B. variegata*, near Cracow in southern Poland. Evolution 40:1141–1159.

Twomey, E., J. S. Vestergaard, and K. Summers. 2014*a*. Reproductive isolation related to mimetic divergence in the poison frog *Ranitomeya imitator*. Nature Communications 5:1–8.

———. 2014*b*. Data from: Reproductive isolation related to mimetic divergence in the poison frog *Ranitomeya imitator*. Nature Communications 5:1–8, Dryad Digital Repository, http://dx.doi.org/10.5061/dryad.rd586.

Twomey, E., J. S. Vestergaard, P. J. Venegas, and K. Summers. 2016. Data from: Mimetic divergence and the speciation continuum in the mimic poison frog *Ranitomeya imitator*. American Naturalist, Dryad Digital Repository, http://dx.doi.org/10.5061/dryad.95tv3.

Twomey, E., J. Yeager, J. L. Brown, V. Morales, M. Cummings, and K. Summers. 2013. Phenotypic and genetic divergence among poison frog populations in a mimetic radiation. PLoS ONE 8:e55443. doi: 10.1371/journal.pone.0055443.

van Oosterhout, C., W. F. Hutchinson, D. P. Wills, and P. Shipley. 2004. MICRO-CHECKER: software for identifying and correcting genotyping errors in microsatellite data. Molecular Ecology Notes 4:535–538.

Wang, I. J. 2013. Examining the full effects of landscape heterogeneity on spatial genetic variation: a multiple matrix regression approach for quantifying geographic and ecological isolation. Evolution 67:3403–3411.

Wang, I. J., and K. Summers. 2010. Genetic structure is correlated with phenotypic divergence rather than geographic isolation in the highly polymorphic strawberry poison-dart frog. Molecular Ecology 19:447–458.

Willink, B., A. García-Rodríguez, F. Bolaños, and H. Pröhl. 2014. The interplay between multiple predators and prey colour divergence. Biological Journal of the Linnean Society 113:580–589.

Yeager, J. 2009. Quantification of resemblance in a mimetic radiation. MS thesis, East Carolina University, Greenville, NC.

Yeager, J., J. L. Brown, V. Morales, M. Cummings, and K. Summers. 2012. Testing for selection on color and pattern in a mimetic radiation. Current Zoology 58:667–675.

Associate Editor: J. Albert C. Uy
Editor: Susan Kalisz